JACS
JOURNAL OF THE AMERICAN CHEMICAL SOCIETY

Article

pubs.acs.org/JACS

Electronic Origins of the Variable Efficiency of Room-Temperature Methane Activation by Homo- and Heteronuclear Cluster Oxide Cations $[XYO_2]^+$ (X, Y = Al, Si, Mg): Competition between Proton-Coupled Electron Transfer and Hydrogen-Atom Transfer

Jilai Li,[†,‡] Shaodong Zhou,[†] Jun Zhang,[§] Maria Schlangen,[†] Thomas Weiske,[†] Dandamudi Usharani,[⊥] Sason Shaik,*[,∥] and Helmut Schwarz*[,†]

[†]Institut für Chemie, Technische Universität Berlin, Straße des 17. Juni 135, 10623 Berlin, Germany

[‡]Institute of Theoretical Chemistry, Jilin University, Changchun 130023, People's Republic of China

[§]Institute of Theoretical Chemistry, University of Cologne, Greinstraße 4, 50939 Cologne, Germany

[⊥]Department of Lipid Science, CSIR-Central Food Technological Research Institute, Mysore 570 020, India

[∥]Institute of Chemistry and the Lise-Meitner-Minerva Center for Computational Quantum Chemistry, The Hebrew University of Jerusalem, 91904 Jerusalem, Israel

Supporting Information

ABSTRACT: The reactivity of the homo- and heteronuclear oxide clusters $[XYO_2]^+$ (X, Y = Al, Si, Mg) toward methane was studied using Fourier transform ion cyclotron resonance mass spectrometry, in conjunction with high-level quantum mechanical calculations. The most reactive cluster by both experiment and theory is $[Al_2O_2]^{\bullet+}$. In its favorable pathway, this cluster abstracts a hydrogen atom by means of proton-coupled electron transfer (PCET) instead of following the conventional hydrogen-atom transfer (HAT) route. This mechanistic choice originates in the strong Lewis acidity of the aluminum site of $[Al_2O_2]^{\bullet+}$, which cleaves the C−H bond heterolytically to form an Al−CH_3 entity, while the proton is transferred to the bridging oxygen atom of the cluster ion. In addition, a comparison of the reactivity of heteronuclear and homonuclear oxide clusters $[XYO_2]^+$ (X, Y = Al, Si, Mg) reveals a striking doping effect by aluminum. Thus, the vacant s−p hybrid orbital on Al acts as an acceptor of the electron pair from methyl anion (CH_3^-) and is therefore eminently important for bringing about thermal methane activation by PCET. For the Al-doped cluster ions, the spin density at an oxygen atom, which is crucial for the HAT mechanism, acts here as a spectator during the course of the PCET mediated C−H bond cleavage. A diagnostic plot of the deformation energy vis-à-vis the barrier shows the different HAT/PCET reactivity map for the entire series. This is a strong connection to the recently discussed mechanism of oxidative coupling of methane on magnesium oxide surfaces proceeding through Grignard-type intermediates.

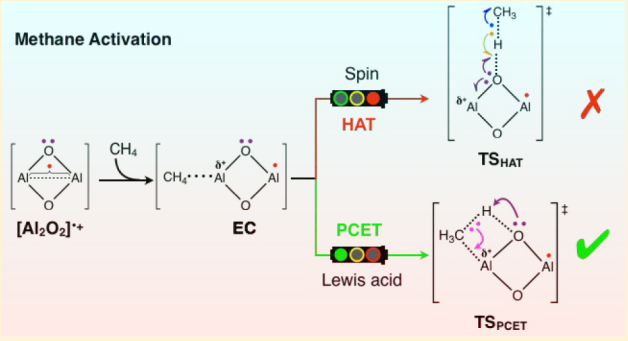

1. INTRODUCTION

Methane constitutes the major component of natural gas and is regarded as an attractive building block for C1 chemistry. However, breaking the thermodynamically strong and kinetically inert C−H bond of CH_4 is viewed as the decisive step in methane conversion. Understanding the underlying mechanisms and improving existing procedures continue to form a major challenge in catalysis and beyond.[1−5]

While it is well accepted that spin density plays a crucial role in the gas-phase chemistry of open-shell metal oxide clusters, in particular with respect to hydrogen-atom transfer (HAT) from methane,[6−13] the nature of the active metal-oxide surface species in heterogeneous catalysis is under fierce debate.[14−18] In an exhaustive review by Zavyalova et al.,[16] covering more than 2700 research articles and about 140 patents on the topic of oxidative coupling of methane by metal oxides, it was concluded that "the real structure of Li/MgO, the nature of the active center and the structure-activity relationship remain unclear, despite all the research that has been done".[16] However, in the gas phase numerous, well-defined cationic oxide clusters containing oxygen-centered radicals are capable of abstracting a hydrogen atom under ambient conditions via *homolytic* C−H bond scission.[6,7,19,20] Examples include simple diatomic transition-metal or main-group element oxides as well as larger cluster ions, for example, $[MgO]^{\bullet+}$,[21] $[CuO]^{\bullet+}$,[22] $[Al_2O_7]^{\bullet+}$,[23] $[(Al_2O_3)_x]^{\bullet+}$ (x = 3−5),[20] $[V_4P_{10}]^{\bullet+}$,[24] $[P_4O_{10}]^{\bullet+}$,[25] $[Ga_2Mg_2O_5]^{\bullet+}$,[26] and $[YAlO_3]^{\bullet+}$.[19] Generally,

Received: April 14, 2016
Published: May 30, 2016

DOI: 10.1021/jacs.6b03798
J. Am. Chem. Soc. 2016, 138, 7973−7981

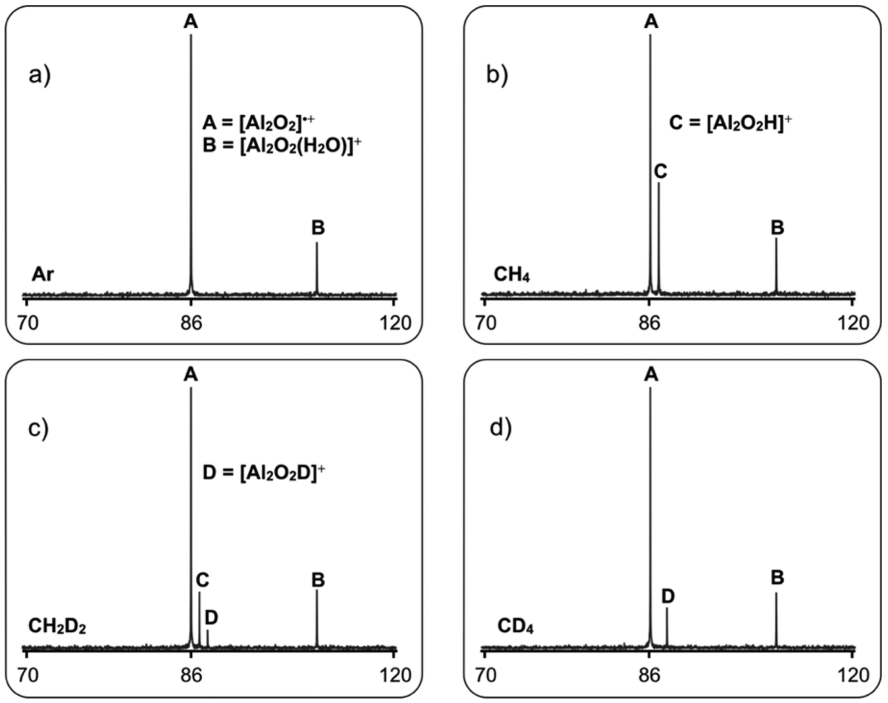

Figure 1. Mass spectra showing the reactivity in the thermal reactions of $[Al_2O_2]^{\bullet+}$ with (a) argon, (b) CH_4, (c) CH_2D_2, and (d) CD_4 at a pressure of 4.0×10^{-9} mbar after a reaction delay of 5 s. The unit for the *x* axes corresponds for all spectra to *m*/*z*. See text for details.

the more reactive cluster ions are those having a localized unpaired electron on one of the oxygen atoms (hence, an oxyl species[9]). However, according to the VB-diagram model, even closed-shell species may abstract a hydrogen atom from hydrocarbons, but in doing so they eventually must undergo additional electronic reorganization to create along the reaction coordinate a radical species at the site of abstraction.[9,27] As a consequence, higher activation barriers will result,[5,7] unless the system can bypass HAT and proceed via the lower energy alternative, proton-coupled electron transfer (PCET).[7,9,27−52]

Metal oxides, capable of bringing about thermal activation of methane in the gas phase,[26,53] are regarded as prototypical systems of active sites in heterogeneous catalysis, the so-called "aristocratic atoms".[54,55] Aluminum-oxide clusters are of special interest because γ-Al_2O_3 has been broadly used as a catalyst in the context of C−H bond activation or as catalyst support in many industrial applications; this is due to its versatile catalytic activity and its high thermal and hydrothermal stability, as well as the low cost.[56−59]

Indeed, gas-phase studies on structurally well-defined metal oxide clusters are considered to serve as ideal models to probe the active site of a catalyst and can provide valuable clues as to mechanistic insight at a molecular level.[1−3,6−10,60−63] In this article, we report the thermal activation of methane mediated by the oxide cluster ions $[XYO_2]^+$ (X, Y = Al, Si, Mg) and investigated by Fourier transform-ion cyclotron resonance (FT-ICR) experiments in conjunction with high-level quantum mechanical (QM) calculations. This combination permits the identification of the elementary steps of C−H bond activation at a strictly molecular level. The thorough comparison of the reactions of methane with both homo- and heteronuclear oxide clusters $[XYO_2]^+$ (X, Y = Al, Si, Mg) turned out to be rather informative with regard to the role of doping effects brought out by the aluminum atom in the cluster. In addition, this gas-phase work reveals an unexpected mechanistic resemblance with the recently suggested *heterolytic* bond cleavage of methane[14,15] at MgO surfaces in the context of oxidative coupling of methane.[16,64−68]

2. RESULTS AND DISCUSSION

The FT-ICR mass spectra, Figure 1, represent the reactions of mass-selected, properly thermalized $[Al_2O_2]^{\bullet+}$ ions (m/z = 86) with isotopologues of methane; spectra of the reactions with background impurities as well as with argon as an inert substrate have also been recorded to serve as a reference. As shown in Figure 1a, when only argon was introduced in the ICR cell, a signal with Δm = +18 relative to the precursor ion $[Al_2O_2]^{\bullet+}$ appears, which can be assigned to the product ion $[Al_2O_2(H_2O)]^{\bullet+}$, indicating that $[Al_2O_2]^{\bullet+}$ reacts with background water.[26,69,70] When CH_4 was admitted to the ICR cell at a stationary pressure of 4.0×10^{-9} mbar, a signal due to hydrogen-atom transfer (HAT) from methane can clearly be identified as $[Al_2O_2H]^+$, Figure 1b. The C−H bond scission was confirmed in isotopic labeling experiments with CD_4: only $[Al_2O_2D]^+$ is generated with the concomitant elimination of $CD_3^{\bullet}$, Figure 1d. The compositions of all the product ions $[Al_2O_2(H_2O)]^{\bullet+}$, $[Al_2O_2H]^+$, and $[Al_2O_2D]^+$ have been confirmed in high-resolution measurements.

The rate constant for this process, $k([Al_2O_2]^{\bullet+}/CH_4)$, is estimated to be 1.1×10^{-10} cm^3 molecule^{-1} s^{-1}, corresponding to a collision efficiency of ϕ = 10.3%, relative to the collision rate.[71−73] Thus, the reaction of the oxygen-deficient oxide cluster $[Al_2O_2]^{\bullet+}$ with methane is slightly more efficient than that of the $[Al_2O_3]^{\bullet+}/CH_4$ couple (ϕ = 7%), which bears a terminal $O^{\bullet}$ radical.[74] The intramolecular kinetic isotope effect (KIE) derived from the $[Al_2O_2]^{\bullet+}/CH_2D_2$ couple amounts to KIE = 2.9, Figure 1c.

To obtain mechanistic insight into the $[Al_2O_2]^{\bullet+}$ mediated hydrogen-atom abstraction from methane, high-level QM

DOI: 10.1021/jacs.6b03798
J. Am. Chem. Soc. 2016, 138, 7973−7981

calculations were carried out. The corresponding potential energy surfaces (PESs) are shown in Figure 2.

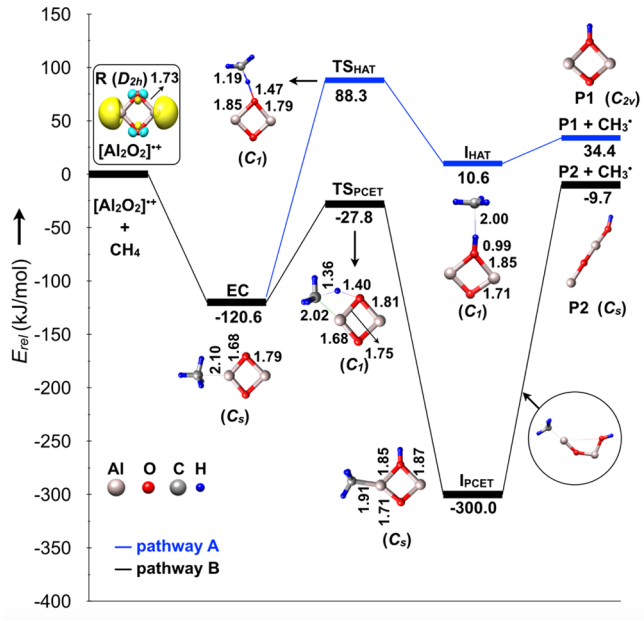

Figure 2. Potential energy profiles for the reaction of $[Al_2O_2]^{\bullet+}$ with CH_4 at the CCSD(T)/CBS[AVTZ:AVQZ]//B2GP-PLYP/def2-TZVP level of theory. Key bond lengths (Å) are also given. The inset shows the ground-state structure of $[Al_2O_2]^{\bullet+}$. The yellow and cyan lobe-isosurfaces indicate the NBO-calculated spin density distributions. Charges are omitted for the sake of clarity.

The most stable structure of $[Al_2O_2]^{\bullet+}$ corresponds to a rhombus-like geometry[75] with the spin density evenly distributed over the two aluminum atoms (Figure 2, R). For the reaction of $[Al_2O_2]^{\bullet+}$ with CH_4, two reaction paths, A and B, were located on the doublet ground state surface (Figure 2). Both paths start with the formation of an encounter complex, EC, from the reactants R and CH_4; this barrier-free step is exothermic by 121 kJ mol^{-1}. Notably, EC is significantly stabilized by an electrostatic interaction between the Lewis acidic aluminum (δ^+) coordination site and the Lewis basic carbon atom (δ^-) of methane.

Let us consider first the conventional hydrogen atom transfer, pathway A in Figure 2. Since the spin is localized on the Al atoms, one might have thought that they would abstract a H atom. This is however not the case since $Al^{\bullet}$ is a poor H-abstractor due to unfavorable thermodynamics. Indeed, the calculations indicate that the energy of the system invariably goes up during a hydrogen-atom transfer from methane to the Al atom, and this process is rather endothermic by 120 kJ mol^{-1} higher in energy relative to the separated reactants. Thus, we omitted it from Figure 2 for the sake of simplicity and considered HAT by the bridging oxygen. However, since the spin is not located on O, the $[Al_2O_2]^{\bullet+}$ cluster has to undergo electron reorganization to create an O-centered spin, for which it will have to pay a penalty of a high barrier.[9,27] Indeed, as shown in the blue energy profile in Figure 2, the HAT starting from EC to I_{HAT} via TS_{HAT} is not accessible under thermal conditions because the reaction is associated with a barrier that is located 88 kJ mol^{-1} higher in energy than the entrance channel. The structures of the stationary points along pathway A closely resemble those of a radical mechanism described before for HAT processes.[6,7,9,26,27,53,69]

However, in pathway B, starting from EC, a C−H bond is cleaved and the hydrogen atom is transferred to the bridging oxygen atom via transition state TS_{PCET}; the latter is located 28 kJ mol^{-1} below the separated reactants. This process results in the formation of a rather stable intermediate I_{PCET} that lies below the reaction entrance by 300 kJ mol^{-1}. To generate the HAT products, the methyl group dissociates from the cluster.

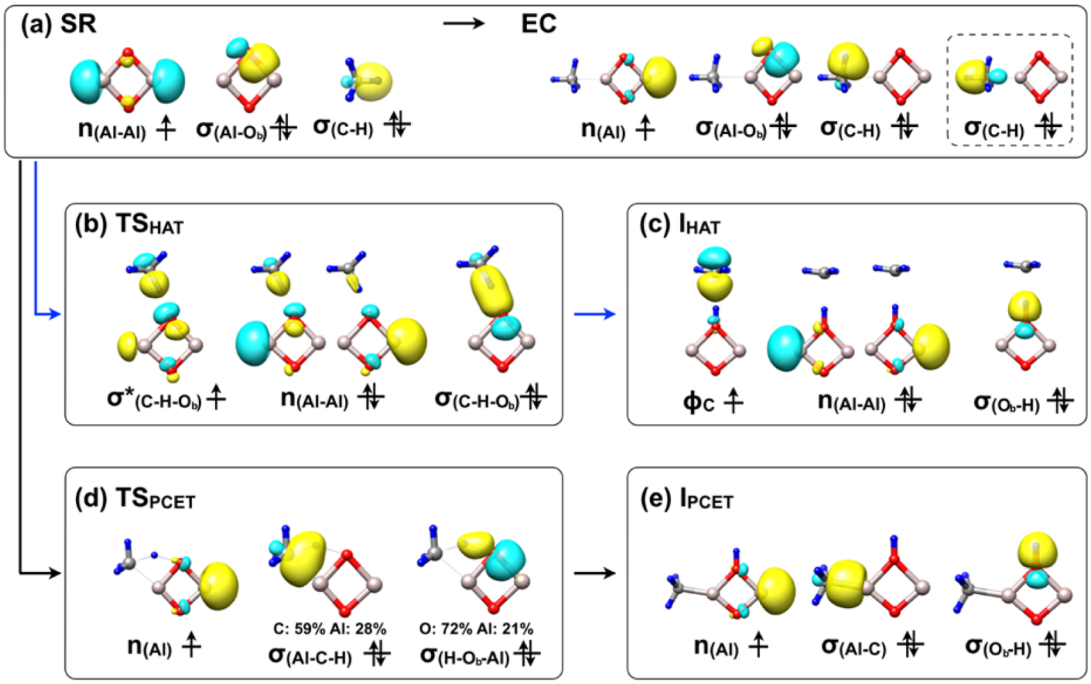

Figure 3. Schematic frontier molecular orbital diagrams represented by QROs (quasi-restricted orbitals) for the HAT (blue) and PCET (black) processes.

DOI: 10.1021/jacs.6b03798
J. Am. Chem. Soc. 2016, 138, 7973−7981

This process takes place along with the opening of the $[Al_2O_2]$ ring thus forming the linear-shaped hydroxide product ion P2. Pathway B can be described as a *heterolytic* cleavage of the C−H bond (of methane) by the Al^+-O^- bond of the cluster. The rate-determining step corresponds to the activation of the C−H bond via transition state TS_{PCET}. Thus, the basic oxygen moiety abstracts hydrogen as a proton, while the CH_3 moiety moves with the electron pair, as CH_3^-, and makes a bond with the positively charge Al^+, as such forming two new bonds, O−H and Al−CH_3 (I_{PCET}). This mechanistic scenario of C−H bond activation is in line with the KIE measured in the experiments.

To provide further details and insight, we performed an analysis of the orbitals that participate in the chemical transformation.[53,69,76−81] Figure 3 shows the detailed evolution of the electronic structures along the two reaction pathways, A and B.

Pathway A can be described in terms of a standard hydrogen-atom transfer mechanism. As shown in Figure 3a, initially, the reactants possess a singly occupied orbital distributed over the two Al atoms, $n_{(Al-Al)}$, and a $\sigma_{(Al-O_b)}$ orbital that represents one of the bridging Al−O bonds, and finally the third orbital corresponds to $\sigma_{(C-H)}$ of the bond undergoing cleavage. At the EC intermediate, the electron-spin undergoes localization on a single Al and resides in the singly occupied $n_{(Al)}$ orbital. The other Al moiety becomes cationic and binds to the substrate methane by exerting significant electrostatic interactions (Figure 3a, inset). In Figure 3b, at the TS_{HAT} species, there is a major electronic reorganization; the $n_{(Al-Al)}$ orbital of the Al···Al moiety becomes doubly occupied (shown by the coupled spin orbitals in the center) as the β electron migrated from the oxygen atom O_b; the residual α electron is used to form the new O_b−H bond, and the radical occupies now an antisymmetric orbital ($\sigma^*_{(C-H-O_b)}$) composed of the lobes on H_3C and O_b. Also depicted is the doubly occupied bonding orbital, $\sigma_{(C-H-O_b)}$, such that there are three electrons delocalized over the C−H−O_b moiety in TS_{HAT}. In Figure 3c, at the intermediate I_{HAT}, the cluster has an O_b−H bond described by the $\sigma_{(O_b-H)}$ orbital, and the radical is located at the weakly coordinated CH_3 moiety in ϕ_C. These features are consistent with a conventional HAT pathway, which is steered by an electronic reorganization that shifts the unpaired electron from the Al···Al moiety to the oxygen atom O_b, while paying the energetic price in terms of a high-energy TS_{HAT} species. Note that the NBO spin and charge developments along the reaction coordinates also support the above analysis (see Table 1). The electronic reorganization during C−H bond cleavage is summarized in Scheme 1.

In contrast, pathway B has the features of a *heterolytic* cleavage of a C−H bond of methane via a proton-coupled electron transfer. Thus, as shown in Figure 3d, the electron pair residing in the $\sigma_{(C-H)}$ bond of methane interacts with an empty s−p orbital of the Al atom to which methane coordinates and forms a three centered orbital, $\sigma_{(Al-C-H)}$. Further, the remaining proton interacts with the doubly occupied $\sigma_{(Al-O_b)}$ orbital of a bridging oxygen atom (O_b). Thus, in the I_{PCET} complex, a $\sigma_{(O_b-H)}$ bond and a $\sigma_{(Al-C)}$ bond are created; in the former the two electrons originate from the doubly occupied $\sigma_{(Al-O_b)}$ orbital and in the latter from the $\sigma_{(C-H)}$ bond of methane.[9] Note that the unpaired electron that was initially delocalized over the two Al atoms in the precursor ion R is shifted in the encounter complex EC as well as in TS_{PCET} and intermediate

Table 1. NBO Spin and Charge Development along the Reaction Coordinates in the PCET and HAT Pathways of the $[Al_2O_2]^{\bullet+}/CH_4$ Couple[a]

	SR	EC	TS_{HAT}	I_{HAT}	TS_{PCET}	I_{PCET}
			Spin			
Al_a	0.56	0.03	0.87	−0.90	0.00	0.00
Al	0.56	0.92	−0.78	0.90	0.92	0.93
O_b	−0.06	0.02	0.45	0.03	0.03	0.03
O	−0.06	0.02	0.03	0.00	0.03	0.04
C	0.00	0.00	0.42	1.04	0.02	0.01
H_t	0.00	0.00	0.01	0.02	0.00	0.00
			Charge			
Al_a	1.93	2.12	1.60	1.62	2.13	2.07
Al	1.93	1.62	1.73	1.62	1.62	1.64
O_b	−1.43	−1.45	−1.21	−1.32	−1.42	−1.28
O	−1.43	−1.45	−1.47	−1.51	−1.43	−1.48
C	−0.99	−1.05	−0.60	−0.49	−1.29	−1.28
H_t	0.25	0.29	0.29	0.54	0.47	0.55

[a]SR, isolated oxide cluster and substrate; EC, encounter complex; TS_{PCET}, transition state in the PCET pathways; TS_{HAT}, transition state in the HAT pathways. Al_a, the active site; Al, the spectator aluminum; O_b, the hydrogen abstracting atom; O, the spectator oxygen; H_t, the transferring hydrogen.

Scheme 1. Schematic Electron Transfers during HAT and PCET Pathways[a]

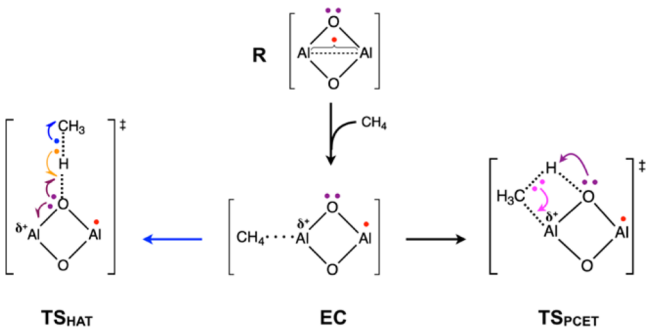

[a]Lone pair electrons not involved in the reaction are omitted for the sake of clarity.

I_{PCET} to the Al atom opposite to the Al coordination site for methane. Indeed, the analysis of NBO spin and charge distribution (Table 1) indicates that the unpaired electron is not located on the hydrogen abstracting oxygen atom O_b, and significant negative charge accumulates at the oxygen atom O_b and carbon atom in TS_{PCET}; the O_b charge facilitates the C−H bond activation by proton abstraction, and the carbon charge is beneficial to the creation of an Al−CH_3 bond (Scheme 1). In addition, with an Al−C covalent bond being formed in TS_{PCET} compared with the unfavorable 3*e*/3c bond in TS_{HAT}, the former TS lies much lower in energy than the latter. Therefore, pathway B is favored over pathway A.

In addition to $[Al_2O_2]^{\bullet+}$, the related oxide clusters $[Mg_2O_2]^{\bullet+}$[21] and $[Si_2O_2]^{\bullet+}$[82] have also been studied with respect to their reactivity toward small alkanes. As described previously,[21] $[Mg_2O_2]^{\bullet+}$ activates propane and butane in single and double HAT reactions. According to our experimental observations, $[Mg_2O_2]^{\bullet+}$ is also capable of abstracting up to two hydrogen atoms from ethane, while $[Si_2O_2]^{\bullet+}$ reacts only slowly with propane at ambient conditions under 3-fold HAT (for details, see Figures S1−S5 in Supporting Information, SI).

DOI: 10.1021/jacs.6b03798
J. Am. Chem. Soc. 2016, 138, 7973−7981

Scheme 2. Schematic Presentation for the HAT and the PCET Pathways from Methane Mediated by Homo- and Heteronuclear Metal Oxide Clusters Studied Computationally

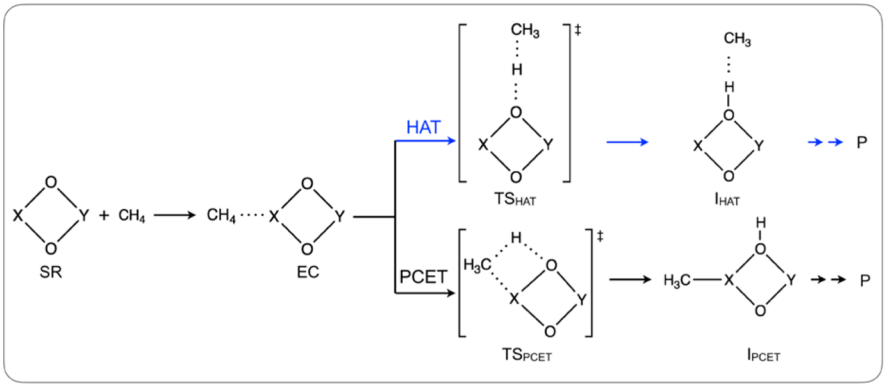

However, neither of these two clusters reacts with methane. Thus, the oxide cluster ions $[Mg_2O_2]^{\bullet+}$, $[Si_2O_2]^{\bullet+}$, and $[Al_2O_2]^{\bullet+}$ exhibit quite distinct reactivity patterns toward small hydrocarbons.

It is well-known that doped oxide clusters permit one to address some of the fundamental challenges related to, for example, the conversion of hydrocarbons.[6,26,60] Therefore, we systematically studied the activation of methane for the series of both homo- and heteronuclear oxide cluster ions $[XYO_2]^+$ (X, Y = Mg, Al, Si, Scheme 2) by computational methods. For all species, both pathways have been located, that is, the conventional HAT reaction involving a transition structure with a linear arrangement of the O−H−C atoms (TS_{HAT}) and the PCET reaction (TS_{PCET}), possessing features of a σ bond heterolytic addition corresponding to an insertion of a $[X^+-O^-]$ unit into the C−H bond of methane (Scheme 2). The NBO charges and spin density distributions are shown in Tables S1 and S2, respectively. The relative energies are given in Table S3.

For all PCET pathways of the $[XYO_2]^+/CH_4$ systems considered in this study, the spin density on the transferring hydrogen atom, H_t, is zero, except for the $[MgSiO_2]^+/CH_4$ system, in which a negligible spin density of 0.01|e| at H_t has been calculated. Furthermore, the negative charge on the carbon atom increases significantly from −0.99 in free methane to values ranging from −1.16 to −1.34 in TS_{PCET} (Table S1), indicating that in the PCET reaction electron density is transferred to the carbon atom as outlined in Scheme 1. Regarding the spin density distribution of the HAT pathway (Table S2), only the oxide cluster $[Mg_2O_2]^{\bullet+}$ possesses a significant spin density at O_b, and as expected, the corresponding barrier for the HAT reaction, TS_{HAT}, is consequently lower in energy (15 kJ mol^{-1}) than the TS_{HAT} of the other systems investigated for which they cover a range from 97 to 124 kJ mol^{-1} with respect to separated reactants (Table S3).

To understand the HAT/PCET dichotomy, we examined in Figure 4 a map of the deformation energy (ΔE_{def}) vs the respective barrier ($\Delta E^{\ddagger}$) for all the reactions studied herein using the energy decomposition analysis.[83−93] The barrier is related to the deformation energy as follows:

$$\Delta E^{\ddagger} = \Delta E_{def} + \Delta E_{int}$$

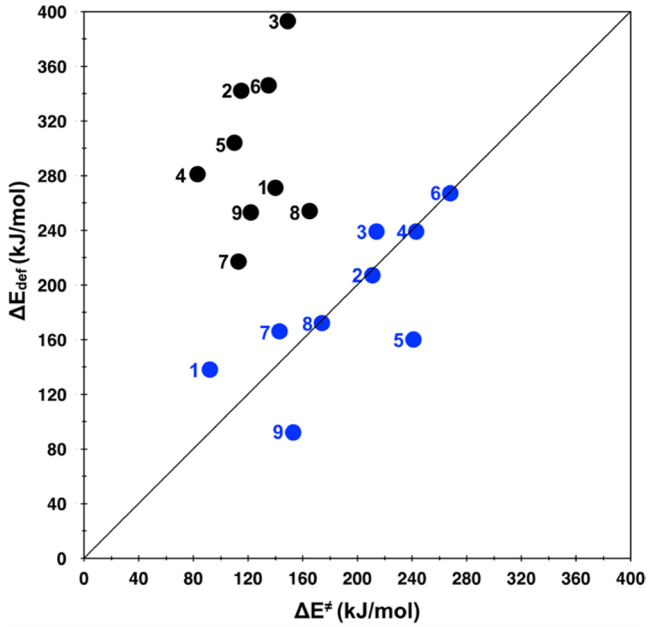

Figure 4. A plot of the sum of the deformation energies of the reactants in the TS (ΔE_{def}, kJ mol^{-1}) vs the corresponding barriers $\Delta E^{\ddagger}$ (kJ mol^{-1}) relative to the encounter complexes, for the reactions of systems R1−R9 (Scheme 2). The line is drawn with a slope of unity such that $\Delta E_{def} = \Delta E^{\ddagger}$ while the vertical distance from the line gauges the interaction energy between the deformed reactants at the TSs. The black spheres correspond to the PCET pathways, while the blue spheres correspond to the HAT pathways.

ΔE_{int} is the total interaction energy, contributed by repulsive interactions (e.g., Pauli repulsion) and stabilizing interactions (electrostatic, polarization, and bonding). As noted by some of us (S.S. and U.D.) in the past, Figure 4 serves as diagnostic of the HAT/PCET dichotomy.[94] The line in the figure has a slope of unity and is the location where $\Delta E^{\neq} = \Delta E_{def}$. It is seen that for most of the HAT reactions (blue spheres) the barriers cluster close to the line and, hence, are close to the deformation energies, such that the barrier derives largely from the deformation energy.[94,95] By contrast, in all the PCET reactions (black spheres), the ΔE_{def} is much larger than the barrier, whereas the interaction energy compensates for this high deformation and lowers the barriers well below the

DOI: 10.1021/jacs.6b03798
J. Am. Chem. Soc. 2016, 138, 7973−7981

corresponding HAT reaction. These significant stabilizing interactions in the TS_{PCET} reflect its multicentered bonding as well as its highly ionic character, which brings about electrostatic stabilization and thus stabilizes the transition state for PCET pathways.[94,95]

Among the various clusters, those with X = Al, that is, all systems in which methane coordinates to an Al atom (R4 and R5, Table S3), are more reactive than the other congeners with respect to the PCET reactions. Further, prohibitively high barriers are encountered for pathways in which Si serves as an active site. Overall, the most reactive cluster for PCET corresponds to the closed-shell cluster ion $[AlMgO_2]^+$ in which the Al atom acts as the active site.

What are the particular properties of aluminum that facilitate methane activation mediated by the oxide clusters $[XYO_2]^+$ (X, Y = Mg, Al, Si) via a PCET reaction? In general, the formation of rather stable encounter complexes and intermediates can pull the barrier below the entrance channel. For the systems investigated in this study, the relative energies of the rate-limiting transition states are controlled by the Lewis acidity of the metal M (M = Al, Si, Mg) and the Lewis basicity of the oxygen atom (O_b) of the active sites.[61,96] Al can form three covalent bonds; further, as a Lewis acidic metal, the cluster is electron-deficient and the Al atom possesses an empty orbital. Thus, in these PCET pathways in which Al serves as the active site, the clusters favor the *heterolytic* cleavage of the C−H bond (Scheme 1). When Mg serves as active site, the formation of a Mg−C bond is expected to be relatively unfavorable since only two ionic bonds can be formed for Mg. For instance, for the cluster ions $[MgAlO_2]^+$ and $[MgSiO_2]^+$, the formation of the Mg−C bond is associated with a cleavage of the Mg−O bond, and for $[Mg_2O_2]^+$, the Mg−O bond is significantly elongated. Regarding the Si containing oxides, this element can form a σ and a π bond to O_b, rather than the single Al−O_b σ bond in the Al containing oxides and the ionic Mg−O_b bond in the oxides consisting of Mg. Therefore, when Si serves as active site, a π-bond between Si and O_b has to be broken in the metathesis process. This causes the Si atom to undergo an $sp^2 \rightarrow sp^3$ hybridization transition and shifts the dihedral angle of the methyl group out of the Si_2O_2 ring. This process requires a significant promotion energy. Moreover, the newly generated $O^\bullet$ and $Si^\bullet$ radicals do not favor a PCET but a HAT reaction.

In the $[AlMgO_2]^+$ species (R4), the Lewis acid character of Al for the *heterolytic* cleavage of the C−H bond of methane is supported by the ionic character of the Mg−O bond. Thus, in contrast to the Si−O bond, which possesses a more covalent character, the oxygen atom O_b of the active site is more electron-rich and can thus serve as a better Lewis base to accept the proton in the PCET reaction. Therefore, the closed-shell cluster ion $[AlMgO_2]^+$ exhibits the lowest transition structure for the PCET reaction as mentioned above. This finding provides an unexpected analogy to the recently reported oxidative coupling of methane on magnesium oxide surfaces proceeding through Grignard-type intermediates generated upon a *heterolytic* cleavage of the C−H bond.[15] More interestingly, the $[Al_2O_2]^{\bullet+}$ unit demonstrates much higher reactivity toward methane with a −28 kJ mol^{-1} activation barrier relative to the reaction entrance, while the $Li^+O^{\bullet-}$ doped magnesium oxides cannot do this job since a significant barrier ranging from 12 to 61 kJ mol^{-1} is unavoidable.[15] Furthermore, these trends are in line with the VB modeling of the PCET/HAT dichotomy.[7,27,94]

3. CONCLUSIONS

In summary, we provide herein mechanistic insight into the activation of methane mediated by the oxide cluster ions $[XYO_2]^+$ (X, Y = Al, Si, Mg). While the homonuclear cluster $[Al_2O_2]^{\bullet+}$ has been investigated by FT-ICR-MS experiments and high-level QM calculations, the reactivity patterns of the other cluster oxides toward methane have only been compared in a theoretical study. $[Al_2O_2]^{\bullet+}$ exhibits a surprisingly high reactivity, and the energetically most favorable pathway exhibits, according to the calculations, features typical of a PCET mechanism instead of a more conventional HAT process. This finding can be ascribed to the strong Lewis acidity of the aluminum site of the cluster ion, which enables the *heterolytic* cleavage of the C−H bond of methane and forms a new Al−CH_3 bond concomitant with a proton transfer to the bridging oxygen atom (O_b) of the cluster (Scheme 1). Further, a comparison of the reactivities of homo- and heteronuclear oxide clusters $[XYO_2]^+$ (X, Y = Al, Si, Mg) predicts a striking doping effect by aluminum. Unlike Mg, which has a $3s^2$ configuration, Al has $3s^23p^1$ and as such it is better suited to give up its 3p electron, become cationic, and make the bridging metal−O bonds sufficiently ionic to participate in a *heterolytic* cleavage of the C−H bond. Accordingly, the presence of an empty s−p orbital accepting the electron pair from methyl anion (CH_3^-) is crucial to bring about thermal methane activation, while the spin density has no effect on the PCET process. A diagnostic plot of the deformation energy vis-à-vis the barrier shows the different HAT/PCET reactivity map for the entire series of reactions (Figure 4).[94]

4. METHODS

4.1. Experimental Details. The ion/molecule reactions were carried out using a Spectrospin-CMS-47X Fourier-transform ion cyclotron resonance (FTICR) mass spectrometer as described elsewhere.[97−99] Briefly, the oxide cluster ion $[M_2O_2]^{\bullet+}$ (M = Al, Si, Mg) cations were produced by laser ablation of magnesium, aluminum, and silicon targets using a Nd:YAG laser (λ = 1064 nm) in the presence of O_2, which is seeded in the helium carrier gas. The ions generated were transferred from the external ion source into the cylindrical ICR-cell, which is positioned in a superconducting magnet field (7.05 T), by using a system of electrostatic potentials and lenses. After proper thermalization by repeatedly pulsing-in argon (ca. 2×10^{-6} mbar), the reactions of mass-selected $[M_2O_2]^{\bullet+}$ were studied by introducing the neutral reactants via a leak valve. As to the double-hydrogen transfer from ethane to the cluster $[Mg_2O_2]^{\bullet+}$ ion, we also study separately the reaction of $[Mg_2O_2H]^{\bullet+}$ with ethane to identify the precursor ions of secondary or higher-order products. A temperature of 298 K for the thermalized clusters has been assumed.[97,99,100]

4.2. Computational Methods. Unless stated otherwise, all calculations were performed with the Gaussian 09 package.[101] The B2GP-PLYP[69,102−104] double hybrid density functional method in conjunction with the triple-ζ quality basis set def2-TZVP[105] were used to optimize the structures of stationary points along the reaction coordinates. Dispersion correction has been added using Grimme's empirical dispersion parameters implemented in Gaussian 09.[106]

Harmonic vibrational frequencies were computed to verify the nature of the stationary points. The minimum structures reported in this paper show only positive eigenvalues of the Hessian matrix, whereas the transition states (TSs) have one negative eigenvalue. Intrinsic reaction coordinate (IRC)[107−110] calculations were also performed to confirm the connection between transition states and intermediates. Single-point energies at the standard CCSD(T)/CBS[AVTZ:AVQZ] levels of theory using the B2GP-PLYP/def2-TZVP structures were also carried out by using Molpro2012.1.[111] Natural bond orbital (NBO)[112−117] calculations were performed to

DOI: 10.1021/jacs.6b03798
J. Am. Chem. Soc. 2016, 138, 7973−7981

obtain further information on selected stationary points along the reaction coordinates. Quasi-restricted orbitals analysis[118,119] were carried out by using ORCA.[120]

Deformation energies (ΔE_{def}) were calculated at the B2GP-PLYP/def2-TZVP level for the transition states of HAT and PCET pathways and were plotted against the respective barriers ($\Delta E^{\ddagger}$) as a diagnostic tool.[94] ΔE_{def} is the energy spent by reactants upon reaching to transition state, namely $\Delta E_{def} = E(CH_4 + [XYO_2]^+$ at TS geometry) − E(EC), while the respective barriers are the electronic barrier without zero-point energy and any thermal corrections. To avoid negative barriers (see Figure 2), the energy of the encounter complex (EC, Figure 2) was used as a reference state.

■ ASSOCIATED CONTENT

Supporting Information

The Supporting Information is available free of charge on the ACS Publications website at DOI: 10.1021/jacs.6b03798.

Additional mass spectra as mentioned in the text, the most-stable rhombus-like structures of $[XYO_2]^+$ (X, Y = Mg, Al, Si), potential energy surfaces of the $[M_2O_2]^{\bullet+}/CH_4$ (M = Mg, Si) and $[Mg_2O_2]^{\bullet+}/C_2H_6$ systems, the spin density and NBO charge development along the reaction coordinates, relative energies (kJ mol^{-1}) of key stationary points on the HAT and PCET pathways of the $[XYO_2]^+/CH_4$ (X, Y = Al, Si, Mg) systems, additional discussion as mentioned in the text, and Cartesian coordinates and absolute energies for all calculated species (PDF)

■ AUTHOR INFORMATION

Corresponding Authors

*Helmut.Schwarz@tu-berlin.de
*sason@yfaat.ch.huji.ac.il

Notes

The authors declare no competing financial interest.

■ ACKNOWLEDGMENTS

This research was sponsored by the Deutsche Forschungsgemeinschaft (DFG), in particular the Cluster of Excellence "Unifying Concepts in Catalysis" (coordinated by the Technische Universität Berlin and funded by the DFG), and the Fonds der Chemischen Industrie. The work at the Hebrew University has been supported by the Israel Science Foundation (ISF Grant 1183/13). Dr. D. Usharani thanks the Lise Meitner-Minerva Center for computational facilities. We thank Dr. Caiyun Geng for helpful comments. This article is dedicated to Professor Bernard Meunier.

■ REFERENCES

(1) Schwarz, H. *Isr. J. Chem.* **2014**, *54*, 1413−1431.
(2) Schwarz, H. *Angew. Chem., Int. Ed.* **2011**, *50*, 10096−10115.
(3) Schröder, D.; Schwarz, H. *Proc. Natl. Acad. Sci. U. S. A.* **2008**, *105*, 18114−18119.
(4) Olah, G. A. *Angew. Chem., Int. Ed.* **2005**, *44*, 2636−2639.
(5) Arndtsen, B. A.; Bergman, R. G.; Mobley, T. A.; Peterson, T. H. *Acc. Chem. Res.* **1995**, *28*, 154−162.
(6) Schwarz, H. *Chem. Phys. Lett.* **2015**, *629*, 91−101.
(7) Dietl, N.; Schlangen, M.; Schwarz, H. *Angew. Chem., Int. Ed.* **2012**, *51*, 5544−5555.
(8) Ding, X.-L.; Wu, X.-N.; Zhao, Y.-X.; He, S.-G. *Acc. Chem. Res.* **2012**, *45*, 382−390.
(9) Lai, W.; Li, C.; Chen, H.; Shaik, S. *Angew. Chem., Int. Ed.* **2012**, *51*, 5556−5578.
(10) Zhao, Y.-X.; Wu, X.-N.; Ma, J.-B.; He, S.-G.; Ding, X.-L. *Phys. Chem. Chem. Phys.* **2011**, *13*, 1925−1938.
(11) Balcells, D.; Clot, E.; Eisenstein, O. *Chem. Rev.* **2010**, *110*, 749−823.
(12) Crabtree, R. H. *Nat. Chem.* **2009**, *1*, 348−349.
(13) Ceyer, S. T. *Science* **1990**, *249*, 133−139.
(14) Sauer, J.; Freund, H.-J. *Catal. Lett.* **2015**, *145*, 109−125.
(15) Kwapien, K.; Paier, J.; Sauer, J.; Geske, M.; Zavyalova, U.; Horn, R.; Schwach, P.; Trunschke, A.; Schlögl, R. *Angew. Chem., Int. Ed.* **2014**, *53*, 8774−8778.
(16) Zavyalova, U.; Holena, M.; Schlögl, R.; Baerns, M. *ChemCatChem* **2011**, *3*, 1935−1947.
(17) Sinev, M. Y.; Fattakhova, Z. T.; Lomonosov, V. I.; Gordienko, Y. A. *J. Nat. Gas Chem.* **2009**, *18*, 273−287.
(18) Catlow, C. R. A.; French, S. A.; Sokol, A. A.; Thomas, J. M. *Philos. Trans. R. Soc., A* **2005**, *363*, 913−936 and references therein.
(19) Ma, J.-B.; Wang, Z.-C.; Schlangen, M.; He, S.-G.; Schwarz, H. *Angew. Chem., Int. Ed.* **2012**, *51*, 5991−5994.
(20) Feyel, S.; Döbler, J.; Höckendorf, R. F.; Beyer, M. K.; Sauer, J.; Schwarz, H. *Angew. Chem., Int. Ed.* **2008**, *47*, 1946−1950.
(21) Schröder, D.; Roithová, J. *Angew. Chem., Int. Ed.* **2006**, *45*, 5705−5708.
(22) Dietl, N.; van der Linde, C.; Schlangen, M.; Beyer, M. K.; Schwarz, H. *Angew. Chem., Int. Ed.* **2011**, *50*, 4966−4969.
(23) Wang, Z.-C.; Weiske, T.; Kretschmer, R.; Schlangen, M.; Kaupp, M.; Schwarz, H. *J. Am. Chem. Soc.* **2011**, *133*, 16930−16937.
(24) Feyel, S.; Döbler, J.; Schröder, D.; Sauer, J.; Schwarz, H. *Angew. Chem., Int. Ed.* **2006**, *45*, 4681−4685.
(25) Dietl, N. P. R.; Engeser, M.; Schwarz, H. *Angew. Chem., Int. Ed.* **2009**, *48*, 4861−4863.
(26) Li, J.; Wu, X.-N.; Schlangen, M.; Zhou, S.; González-Navarrete, P.; Tang, S.; Schwarz, H. *Angew. Chem., Int. Ed.* **2015**, *54*, 5074−5078.
(27) Li, C.; Danovich, D.; Shaik, S. S. *Chem. Sci.* **2012**, *3*, 1903−1918.
(28) Hammes-Schiffer, S. *J. Am. Chem. Soc.* **2015**, *137*, 8860−8871.
(29) Siewert, I. *Chem. - Eur. J.* **2015**, *21*, 15078−15091.
(30) Saouma, C. T.; Mayer, J. M. *Chem. Sci.* **2014**, *5*, 21−31.
(31) Migliore, A.; Polizzi, N. F.; Therien, M. J.; Beratan, D. N. *Chem. Rev.* **2014**, *114*, 3381−3465.
(32) Savéant, J.-M. *Annu. Rev. Anal. Chem.* **2014**, *7*, 537−560.
(33) Layfield, J. P.; Hammes-Schiffer, S. *Chem. Rev.* **2014**, *114*, 3466−3494.
(34) Weinberg, D. R.; Gagliardi, C. J.; Hull, J. F.; Murphy, C. F.; Kent, C. A.; Westlake, B. C.; Paul, A.; Ess, D. H.; McCafferty, D. G.; Meyer, T. J. *Chem. Rev.* **2012**, *112*, 4016−4093.
(35) Cembran, A.; Provorse, M. R.; Wang, C.; Wu, W.; Gao, J. *J. Chem. Theory Comput.* **2012**, *8*, 4347−4358.
(36) Mayer, J. M. *Acc. Chem. Res.* **2011**, *44*, 36−46.
(37) Mayer, J. M. *J. Phys. Chem. Lett.* **2011**, *2*, 1481−1489.
(38) Wenger, O. S. *Chem. - Eur. J.* **2011**, *17*, 11692−11702.
(39) Liu, S.; Ess, D. H.; Schauer, C. K. *J. Phys. Chem. A* **2011**, *115*, 4738−4742.
(40) Warren, J. J.; Tronic, T. A.; Mayer, J. M. *Chem. Rev.* **2010**, *110*, 6961−7001.
(41) Costentin, C.; Robert, M.; Savéant, J.-M. *Acc. Chem. Res.* **2010**, *43*, 1019−1029.
(42) Hammes-Schiffer, S. *Acc. Chem. Res.* **2009**, *42*, 1881−1889.
(43) Siegbahn, P. E. *Acc. Chem. Res.* **2009**, *42*, 1871−1880.
(44) Tishchenko, O.; Truhlar, D. G.; Ceulemans, A.; Nguyen, M. T. *J. Am. Chem. Soc.* **2008**, *130*, 7000−7010.
(45) Chen, X.; Bu, Y. *J. Am. Chem. Soc.* **2007**, *129*, 9713−9720.
(46) Meyer, T. J.; Huynh, M. H. V.; Thorp, H. H. *Angew. Chem., Int. Ed.* **2007**, *46*, 5284−5304.
(47) Huynh, M. H. V.; Meyer, T. J. *Chem. Rev.* **2007**, *107*, 5004−5064.
(48) Skone, J. H.; Soudackov, A. V.; Hammes-Schiffer, S. *J. Am. Chem. Soc.* **2006**, *128*, 16655−16663.
(49) Mayer, J. M. *Annu. Rev. Phys. Chem.* **2004**, *55*, 363−390.
(50) Mayer, J. M.; Hrovat, D. A.; Thomas, J. L.; Borden, W. T. *J. Am. Chem. Soc.* **2002**, *124*, 11142−11147.

DOI: 10.1021/jacs.6b03798
J. Am. Chem. Soc. 2016, 138, 7973−7981

(51) Hammes-Schiffer, S. *Acc. Chem. Res.* **2001**, *34*, 273−281.
(52) Cukier, R. I.; Nocera, D. G. *Annu. Rev. Phys. Chem.* **1998**, *49*, 337−369.
(53) Li, J.; Wu, X.-N.; Zhou, S.; Tang, S.; Schlangen, M.; Schwarz, H. *Angew. Chem., Int. Ed.* **2015**, *54*, 12298−12302.
(54) Taylor, H. S. *J. Phys. Chem.* **1926**, *30*, 145−171.
(55) Taylor, H. S. *Proc. R. Soc. London, Ser. A* **1925**, *108*, 105−111.
(56) Wischert, R.; Laurent, P.; Copéret, C.; Delbecq, F.; Sautet, P. *J. Am. Chem. Soc.* **2012**, *134*, 14430−14449.
(57) Wischert, R.; Copéret, C.; Delbecq, F.; Sautet, P. *Angew. Chem., Int. Ed.* **2011**, *50*, 3202−3205.
(58) Coperet, C. *Chem. Rev.* **2010**, *110*, 656−680.
(59) Larson, J. G.; Hall, W. K. *J. Phys. Chem.* **1965**, *69*, 3080−3089.
(60) Schwarz, H. *Angew. Chem., Int. Ed.* **2015**, *54*, 10090−10100.
(61) Roach, P. J.; Woodward, W. H.; Castleman, A. W.; Reber, A. C.; Khanna, S. N. *Science* **2009**, *323*, 492−495.
(62) Johnson, G. E.; Tyo, E. C.; Castleman, A. W. *Proc. Natl. Acad. Sci. U. S. A.* **2008**, *105*, 18108−18113.
(63) Schröder, D.; Schwarz, H. *Angew. Chem., Int. Ed. Engl.* **1995**, *34*, 1973−1995.
(64) Schwach, P.; Willinger, M. G.; Trunschke, A.; Schlögl, R. *Angew. Chem., Int. Ed.* **2013**, *52*, 11381−11384.
(65) Arndt, S.; Laugel, G.; Levchenko, S.; Horn, R.; Baerns, M.; Scheffler, M.; Schlögl, R.; Schomäcker, R. *Catal. Rev.: Sci. Eng.* **2011**, *53*, 424−514.
(66) Kwapien, K.; Sierka, M.; Döbler, J.; Sauer, J. *ChemCatChem* **2010**, *2*, 819−826.
(67) Lunsford, J. H. *Angew. Chem., Int. Ed. Engl.* **1995**, *34*, 970−980.
(68) Ito, T.; Lunsford, J. H. *Nature* **1985**, *314*, 721−722.
(69) Li, J.; Zhou, S.; Wu, X.-N.; Tang, S.; Schlangen, M.; Schwarz, H. *Angew. Chem., Int. Ed.* **2015**, *54*, 11861−11864.
(70) Li, J.; Wu, X.-N.; Zhou, S.; Tang, S.; Schlangen, M.; Schwarz, H. *Angew. Chem., Int. Ed.* **2015**, *54*, 12298−12302.
(71) Kummerlöwe, G.; Beyer, M. K. *Int. J. Mass Spectrom.* **2005**, *244*, 84−90.
(72) Su, T.; Bowers, M. T. *J. Chem. Phys.* **1973**, *58*, 3027−3037.
(73) Bowers, M. T.; Laudenslager, J. B. *J. Chem. Phys.* **1972**, *56*, 4711−4712.
(74) Wang, Z. C.; Dietl, N.; Kretschmer, R.; Ma, J. B.; Weiske, T.; Schlangen, M.; Schwarz, H. *Angew. Chem., Int. Ed.* **2012**, *51*, 3703−3707.
(75) Ornelas-Lizcano, J. C.; Guirado-López, R. A. *J. Chem. Phys.* **2015**, *142*, 124311.
(76) Sun, X.; Geng, C.; Huo, R.; Ryde, U.; Bu, Y.; Li, J. *J. Phys. Chem. B* **2014**, *118*, 1493−1500.
(77) Sun, X.; Sun, X.; Geng, C.; Zhao, H.; Li, J. *J. Phys. Chem. A* **2014**, *118*, 7146−7158.
(78) Li, J. L.; Zhang, X.; Huang, X. R. *Phys. Chem. Chem. Phys.* **2012**, *14*, 246−256.
(79) Sun, X. L.; Huang, X. R.; Li, J. L.; Huo, R. P.; Sun, C. C. *J. Phys. Chem. A* **2012**, *116*, 1475−1485.
(80) Geng, C. Y.; Ye, S.; Neese, F. *Angew. Chem., Int. Ed.* **2010**, *49*, 5717−5720.
(81) Fukui, K. *Science* **1982**, *218*, 747−754.
(82) Goldberg, N.; Iraqi, M.; Koch, W.; Schwarz, H. *Chem. Phys. Lett.* **1994**, *225*, 404−409.
(83) van Zeist, W.-J.; Bickelhaupt, F. M. *Org. Biomol. Chem.* **2010**, *8*, 3118−3127.
(84) Ess, D. H.; Houk, K. N. *J. Am. Chem. Soc.* **2008**, *130*, 10187−10198.
(85) Legault, C. Y.; Garcia, Y.; Merlic, C. A.; Houk, K. N. *J. Am. Chem. Soc.* **2007**, *129*, 12664−12665.
(86) Ess, D. H.; Houk, K. N. *J. Am. Chem. Soc.* **2007**, *129*, 10646−10647.
(87) Diefenbach, A.; Bickelhaupt, F. M. *J. Phys. Chem. A* **2004**, *108*, 8460−8466.
(88) Mitchell, D. J.; Schlegel, H. B.; Shaik, S. S.; Wolfe, S. *Can. J. Chem.* **1985**, *63*, 1642−1648.
(89) Ziegler, T.; Rauk, A. *Inorg. Chem.* **1979**, *18*, 1558−1565.
(90) Strozier, R. W.; Caramella, P.; Houk, K. N. *J. Am. Chem. Soc.* **1979**, *101*, 1340−1343.
(91) Ziegler, T.; Rauk, A. *Theor. Chim. Acta* **1977**, *46*, 1−10.
(92) Kitaura, K.; Morokuma, K. *Int. J. Quantum Chem.* **1976**, *10*, 325−340.
(93) Morokuma, K. *J. Chem. Phys.* **1971**, *55*, 1236−1244.
(94) Usharani, D.; Lacy, D. C.; Borovik, A. S.; Shaik, S. *J. Am. Chem. Soc.* **2013**, *135*, 17090−17104.
(95) Usharani, D.; Janardanan, D.; Li, C.; Shaik, S. S. *Acc. Chem. Res.* **2013**, *46*, 471−482.
(96) Luo, Z.; Smith, J. C.; Woodward, W. H.; Castleman, A. W. *J. Phys. Chem. Lett.* **2012**, *3*, 3818−3821.
(97) Engeser, M.; Weiske, T.; Schröder, D.; Schwarz, H. *J. Phys. Chem. A* **2003**, *107*, 2855−2859.
(98) Eller, K.; Zummack, W.; Schwarz, H. *J. Am. Chem. Soc.* **1990**, *112*, 621−627.
(99) Eller, K.; Schwarz, H. *Int. J. Mass Spectrom. Ion Processes* **1989**, *93*, 243−257.
(100) Schröder, D.; Schwarz, H.; Clemmer, D. E.; Chen, Y.; Armentrout, P. B.; Baranov, V. I.; Böhme, D. K. *Int. J. Mass Spectrom. Ion Processes* **1997**, *161*, 175−191.
(101) Frisch, M. J.; Trucks, G. W.; Schlegel, H. B.; Scuseria, G. E.; Robb, M. A.; Cheeseman, J. R.; Scalmani, G.; Barone, V.; Mennucci, B.; Petersson, G. A.; Nakatsuji, H.; Caricato, M.; Li, X.; Hratchian, H. P.; Izmaylov, A. F.; Bloino, J.; Zheng, G.; Sonnenberg, J. L.; Hada, M.; Ehara, M.; Toyota, K.; Fukuda, R.; Hasegawa, J.; Ishida, M.; Nakajima, T.; Honda, Y.; Kitao, O.; Nakai, H.; Vreven, T.; Montgomery, J. A., Jr.; Peralta, J. E.; Ogliaro, F.; Bearpark, M.; Heyd, J. J.; Brothers, E.; Kudin, K. N.; Staroverov, V. N.; Kobayashi, R.; Normand, J.; Raghavachari, K.; Rendell, A.; Burant, J. C.; Iyengar, S. S.; Tomasi, J.; Cossi, M.; Rega, N.; Millam, J. M.; Klene, M.; Knox, J. E.; Cross, J. B.; Bakken, V.; Adamo, C.; Jaramillo, J.; Gomperts, R.; Stratmann, R. E.; Yazyev, O.; Austin, A. J.; Cammi, R.; Pomelli, C.; Ochterski, J. W.; Martin, R. L.; Morokuma, K.; Zakrzewski, V. G.; Voth, G. A.; Salvador, P.; Dannenberg, J. J.; Dapprich, S.; Daniels, A. D.; Farkas, O.; Foresman, J. B.; Ortiz, J. V.; Cioslowski, J.; Fox, D. J. *Gaussian 09*, revision D.01; Gaussian, Inc.: Wallingford, CT, 2009.
(102) Li, J.; Zhou, S.; Schlangen, M.; Weiske, T.; Schwarz, H. *ChemistrySelect* **2016**, *1*, 444−447.
(103) Kang, R. H.; Chen, H.; Shaik, S.; Yao, J. N. *J. Chem. Theory Comput.* **2011**, *7*, 4002−4011.
(104) Karton, A.; Tarnopolsky, A.; Lamère, J.-F.; Schatz, G. C.; Martin, J. M. L. *J. Phys. Chem. A* **2008**, *112*, 12868−12886.
(105) Weigend, F.; Ahlrichs, R. *Phys. Chem. Chem. Phys.* **2005**, *7*, 3297−3305.
(106) Grimme, S.; Antony, J.; Ehrlich, S.; Krieg, H. *J. Chem. Phys.* **2010**, *132*, 154104.
(107) Truhlar, D. G.; Gordon, M. S. *Science* **1990**, *249*, 491−498.
(108) Gonzalez, C.; Schlegel, H. B. *J. Phys. Chem.* **1990**, *94*, 5523−5527.
(109) Fukui, K. *Acc. Chem. Res.* **1981**, *14*, 363−368.
(110) Fukui, K. *J. Phys. Chem.* **1970**, *74*, 4161−4163.
(111) Werner, H.-J.; Knowles, P. J.; Knizia, G.; Manby, F. R.; Schütz, M.; Celani, P.; Korona, T.; Lindh, R.; Mitrushenkov, A.; Rauhut, G.; Shamasundar, K. R.; Adler, T. B.; Amos, R. D.; Bernhardsson, A.; Berning, A.; Cooper, D. L.; Deegan, M. J. O.; Dobbyn, A. J.; Eckert, F.; Goll, E.; Hampel, C.; Hesselmann, A.; Hetzer, G.; Hrenar, T.; Jansen, G.; Köppl, C.; Liu, Y.; Lloyd, A. W.; Mata, R. A.; May, A. J.; McNicholas, S. J.; Meyer, W.; Mura, M. E.; Nicklass, A.; O'Neill, D. P.; Palmieri, P.; Peng, D.; Pflüger, K.; Pitzer, R.; Reiher, M.; Shiozaki, T.; Stoll, H.; Stone, A. J.; Tarroni, R.; Thorsteinsson, T.; Wang, M. MOLPRO: A Package of Ab Initio Programs, version 2012.1; http://www.molpro.net.
(112) Reed, A. E.; Curtiss, L. A.; Weinhold, F. A. *Chem. Rev.* **1988**, *88*, 899−926.
(113) Carpenter, J. E.; Weinhold, F. A. *J. Mol. Struct.: THEOCHEM* **1988**, *169*, 41−62.
(114) Reed, A. E.; Weinstock, R. B.; Weinhold, F. A. *J. Chem. Phys.* **1985**, *83*, 735−746.

DOI: 10.1021/jacs.6b03798
J. Am. Chem. Soc. 2016, 138, 7973−7981

(115) Reed, A. E.; Weinhold, F. A. *J. Chem. Phys.* **1985**, *83*, 1736−1740.
(116) Reed, A. E.; Weinhold, F. A. *J. Chem. Phys.* **1983**, *78*, 4066−4073.
(117) Foster, J. P.; Weinhold, F. A. *J. Am. Chem. Soc.* **1980**, *102*, 7211−7218.
(118) Ye, S.; Geng, C.-Y.; Shaik, S.; Neese, F. *Phys. Chem. Chem. Phys.* **2013**, *15*, 8017−8030.
(119) Neese, F. *J. Am. Chem. Soc.* **2006**, *128*, 10213−10222.
(120) Neese, F. *WIREs Comput. Mol. Sci.* **2012**, *2*, 73−78.

DOI: 10.1021/jacs.6b03798
J. Am. Chem. Soc. 2016, 138, 7973−7981